αvβ3 integrin-dependent endothelial cell dynamics in vivo

Paul A. Rupp[1], András Czirók[1,2] and Charles D. Little[1,*]

[1]Department of Anatomy and Cell Biology, University of Kansas Medical Center, 3901 Rainbow Boulevard, Kansas City, KS 66160, USA
[2]Department of Biological Physics, Eötvös University, Pázmány sétány 1A, Budapest, 1117 Hungary
*Author for correspondence (e-mail: clittle@kumc.edu)

Accepted 9 March 2004

Development 131, 2887-2897
Published by The Company of Biologists 2004
doi:10.1242/dev.01160

Summary

A major challenge confronting developmental cell biologists is to understand how individual cell behaviors lead to global tissue organization. Taking advantage of an endothelial cell-specific marker and scanning time-lapse microscopy, we have examined the formation of the primary vascular pattern during avian vasculogenesis. Five types of distinguishable endothelial cell motion are observed during formation of a vascular plexus: (1) global tissue deformations that passively convect endothelial cells; (2) vascular drift, a sheet-like medial translocation of the entire vascular plexus; (3) structural rearrangements, such as vascular fusion; (4) individual cell migration along existing endothelial structures; and (5) cell process extension into avascular areas, resulting in new links within the plexus. The last four types of motion are quantified and found to be reduced in the presence of an αvβ3 integrin inhibitor. These dynamic cell motility data result in new hypotheses regarding primordial endothelial cell behavior during embryonic vasculogenesis.

Movies available online

Key words: Vasculogenesis, Endothelial cells, αvβ3 integrin, Time-lapse, Computational biology, Quail

Introduction

This study was designed to understand how cell dynamics contribute to the de novo assembly of an organ – the primordial embryonic vasculature. It is widely assumed that motility-related cellular activities, such as exertion of traction and compressional forces, shape-change, and migration of cell populations, are the physical means by which tissues and organs are formed. However, our knowledge about the specific mechanisms is limited to a handful of cases, such as hydra regeneration, sea urchin invagination and convergent extension movements during frog gastrulation (Davidson et al., 2002; Keller et al., 2000; Marsden and DeSimone, 2001; Rieu et al., 2000; Shimizu et al., 2002; Wessel and Wikramanayake, 1999; Zhang et al., 2002). Avian vasculogenesis, the formation of a primary vascular pattern from mesodermal-derived precursor cells (angioblasts) prior to blood flow, offers a number of advantages in studying the dynamics of structure emergence in a warm-blooded vertebrate. Vasculogenesis is a relatively simple morphogenic process requiring only one cell type (primordial endothelial) that can be readily observed and manipulated in avian embryos (Drake et al., 1992; Little and Drake, 2000).

The importance of the endothelial cell has long been recognized and there is rich literature documenting a multitude of endothelial cell regulatory pathways and adhesive behaviors, both cell-cell and cell-extracellular matrix (ECM). Even more effort has been expended on drug discovery, with investigators pursuing agents that either promote or prevent tissue vascularization. Arguably, however, the least understood and most important question facing vascular developmental biologists and tissue engineers is what are the general principles guiding morphogenesis of a functionally patterned array of endothelial tubes?

Various hypotheses have been proposed to account for the cell dynamics of vasculogenesis. One suggests that endothelial cells migrate to pre- and well-defined positions following extracellular guidance cues or chemoattractants (Ambler et al., 2001; Cleaver and Krieg, 1998; Poole and Coffin, 1989). Based on in vitro studies, another hypothesis proposes that angioblasts first segregate into randomly placed compact clusters and engage the surrounding ECM fibers. As a result of traction forces, ECM bundles develop, which in turn later route the motile primordial endothelial cells between clusters (Drake et al., 1997; Vernon et al., 1992; Vernon et al., 1995). A mathematical model demonstrated that suitable cell traction forces, without substantial cell migration, are capable of forming polygonal patterns reminiscent of the primary vascular plexus (Manoussaki et al., 1996).

The above concepts stress the importance of cell-ECM interactions during vascular pattern formation. Previous studies have established the importance of the αvβ3 integrin during vessel formation, because in situ inhibition of αvβ3 resulted in abrogation of vascular morphogenesis (Brooks et al., 1994a; Drake et al., 1995). Additionally, tumor and skin graft models showed αvβ3 antagonists promoted tumor regression and apoptosis of angiogenic vessels (Brooks et al., 1994b; Brooks et al., 1995).

Owing to recent improvements in digital microscopy, it is now possible to address directly how blood vessels form de novo (Czirok et al., 2002; Rupp et al., 2003). Scanning time-lapse microscopy and statistical analyses of the recorded biological motion results in a simultaneous tissue- and cellular-

scale characterization of primordial endothelial cell behavior. Here, we have examined how perturbing αvβ3 cell-ECM interactions influenced vascular patterning dynamics. We conclude that subtle, specific alterations in endothelial cell behavior are manifested over time as a highly amplified malformation of the primary vascular plexus.

Materials and methods

Embryo preparation

Quail embryos (*Coturnix coturnix japonica*, Smith Farms, Bucyrus, KS) at Hamburger and Hamilton (HH) stages 8-9 (Hamburger and Hamilton, 1951) were mounted on paper rings to allow their ex ovo manipulation and observation as described by Rupp et al. (Rupp et al., 2003). Intact embryos were placed ventral side up on a 5% agar (PBS) bed for microinjection.

Embryo microinjection

Non-treated embryos were microinjected with Cy3 (Amersham Pharmacia Biotech, Piscataway, NJ) fluorochrome-conjugated QH1 antibody (Cy3-QH1) (Developmental Studies Hybridoma Bank, University of Iowa, Ames, IA) to label quail vascular endothelial cells. Two 25 nl Cy3-QH1 injections (0.58 ng/nl) were introduced bilaterally per embryo into the interstitial space between the endoderm and splanchnic mesoderm. On the basis of several hundred embryos, there is no evidence that microinjection of PBS, human serum albumin, hybridoma 'G' or immunoglobins, per se, interfere with normal embryonic or vascular development, as judged by QH1 staining (Drake et al., 1995; Drake et al., 1992; Drake et al., 2000; Drake and Little, 1991; Drake and Little, 1995) (P.A.R. and C.D.L., unpublished).

Control embryos were injected with a non-function blocking antibody to the αv integrin subunit (MAB1953Z, Chemicon International, Temecula, CA), in addition to Cy3-QH1. MAB1953Z (1 ng/nl) was introduced in four 25 nl microinjections (13 embryos), one 25 nl microinjection at 4 ng/nl (2 embryos) or four 25 nl injections at 4 ng/nl (5 embryos).

Experimentally perturbed embryos were injected with LM609 (MAB1976Z, Chemicon International, Temecula, CA), in addition to Cy3-QH1. MAB1976Z (1 ng/nl) was introduced in four 25 nl microinjections, two per embryonic side, or one 25 nl microinjection at 4 ng/nl (16 embryos total).

Embryo culture

Embryos were cultured as described by Rupp et al. (Rupp et al., 2003). Briefly, injected embryos were placed ventral side up on suture beds within a modified culture chamber containing 3.5 ml Leibovitz-L15 medium supplemented with 2 mM L-glutamine, 10% chick serum and 1% penicillin-streptomycin (GibcoBRL, Grand Island, NY). A second paper ring was placed on top of the embryos, empty wells were filled with sterile deionized H_2O, and the chamber was then sealed shut and positioned on a microscope stage insert within an attached incubator heated to ~38°C.

Image acquisition and movie assembly

Images for time-lapse analysis were acquired on a Leica DMR upright scope (Leica Microsystems, Wetzlar, Germany) with attached Ludl BioPrecision stage (Ludl Electronic Products, Hawthorne, NY). All imaging was carried out using a 10× (0.25 NA) objective with a 20 mm working distance and a Photometrics Quantix cooled CCD camera (Roper Scientific, Tucson, AZ). A complete description of the software for image acquisition and movie assembly is described elsewhere (Czirok et al., 2002). A more complete description of the instrumentation can be found elsewhere (Czirok et al., 2002; Rupp et al., 2003).

In each experiment, images are acquired for three embryos. For each individual embryo, a rectangular area is created from 2×3 slightly overlapping microscopic fields. Multiple (10) focal planes for each field are recorded at 20 μm intervals, first in DIC and immediately thereafter in epifluorescence modes. The acquisition of the '*z*-stack' pairs is accomplished within a short period of time (typically a minute) ensuring the correct spatial registration of the corresponding DIC/epifluorescence image pairs. The practical result of this technology is that every position of the embryonic disc lies within one of the focal planes; thus, no feature is lost or out of focus.

Quantification and compensation of vascular drift

Image alignment was carried out as described in detail previously (Czirok et al., 2002). Briefly, to align an image pair, a pixel-by-pixel comparison is performed for a large number of possible relative offsets. The best alignment is selected as the offset, which results in the least average pixel-by-pixel difference between the shifted image copies.

Embryos change their shape and position considerably during development. To provide an internal frame of reference, DIC images were aligned in such a way that major embryonic features (intersomitic clefts and the notochord) remained stationary in the resulting image sequences. The same translations were implemented onto the epifluorescence image sequences as well, keeping the DIC/epifluorescence image pairs in register.

To quantify and compensate for vascular drift, an initial vascular pattern was selected lateral to the 3rd-6th somites. The movement of the pattern was determined by successive re-alignments performed on the previously motion-compensated image sequences, resulting in a sequence of offset vectors dx_i, where i is the frame index. The cumulative displacement (X_i) of the structure visible in frame i, relative to the steady anatomical features, is then given simply as $X_i=-\sum^{i}_{j=0}dx_j$. Moreover, drift compensation can be achieved by shifting the image on each frame by $-X_i$ (Czirok et al., 2002).

Cell tracking and velocity

Manual tracking, using software described previously, followed the two-dimensional projections of various primordial endothelial cells (PECs) and endothelial structures (Hegedus et al., 2000). Briefly, this software allows tracking the point of interest in x, y and z directions over time. When performed, this procedure resulted in the positions $x_a(t)$ of a certain object a at various time points t. The velocity, $v_a(t)$, was calculated as the net displacement of the geometrical center during 1 hour long time intervals: $v_a(t)=|x_a(t+\Delta t)-x_a(t)|\Delta t$, where $\Delta t=1$ hour.

Average displacement

To describe the persistence of cell motility (Stokes et al., 1991), $d_a(\tau)$, the average distance of migration during a time period of length τ was calculated for each cell a and a wide range of τ, as $d_a(\tau)=\{|x_a(t+\tau)-x_a(t)|\}_t$. For a given value of τ, the average $\{\ldots\}_t$ includes each possible time point t for which both $x_a(t+\tau)$ and $x_a(t)$ exists. In a similar fashion, an entire cell population can be characterized by $d(\tau)=\{|x_a(t+\tau)-x_a(t)|\}_{a,t}$, where averaging extends over each cell of the population in addition to t. The functional form of d is very characteristic for the underlying motion. In the case of a mathematical random walk, d grows as a square root of τ, while for a highly persistent, straight motion d is proportional to τ.

Statistical analysis

Wilcoxon tests with significance level of $P<0.05$ were used to compare the sets of data. This test is insensitive to variations in sample size and does not assume a particular analytical form of the distribution.

Statistical errors of the $d(\tau)$ displacement curves were calculated as $E^2(\tau)=\{d^2_a(\tau)_a-\{d_a(\tau)\}^2_a$. For a fixed τ, the significance of difference between two $d(\tau)$ curves was established by comparing the sets of corresponding $d_a(\tau)$ values. Each of these is characterizing distinct cells and therefore is assumed to be statistically independent.

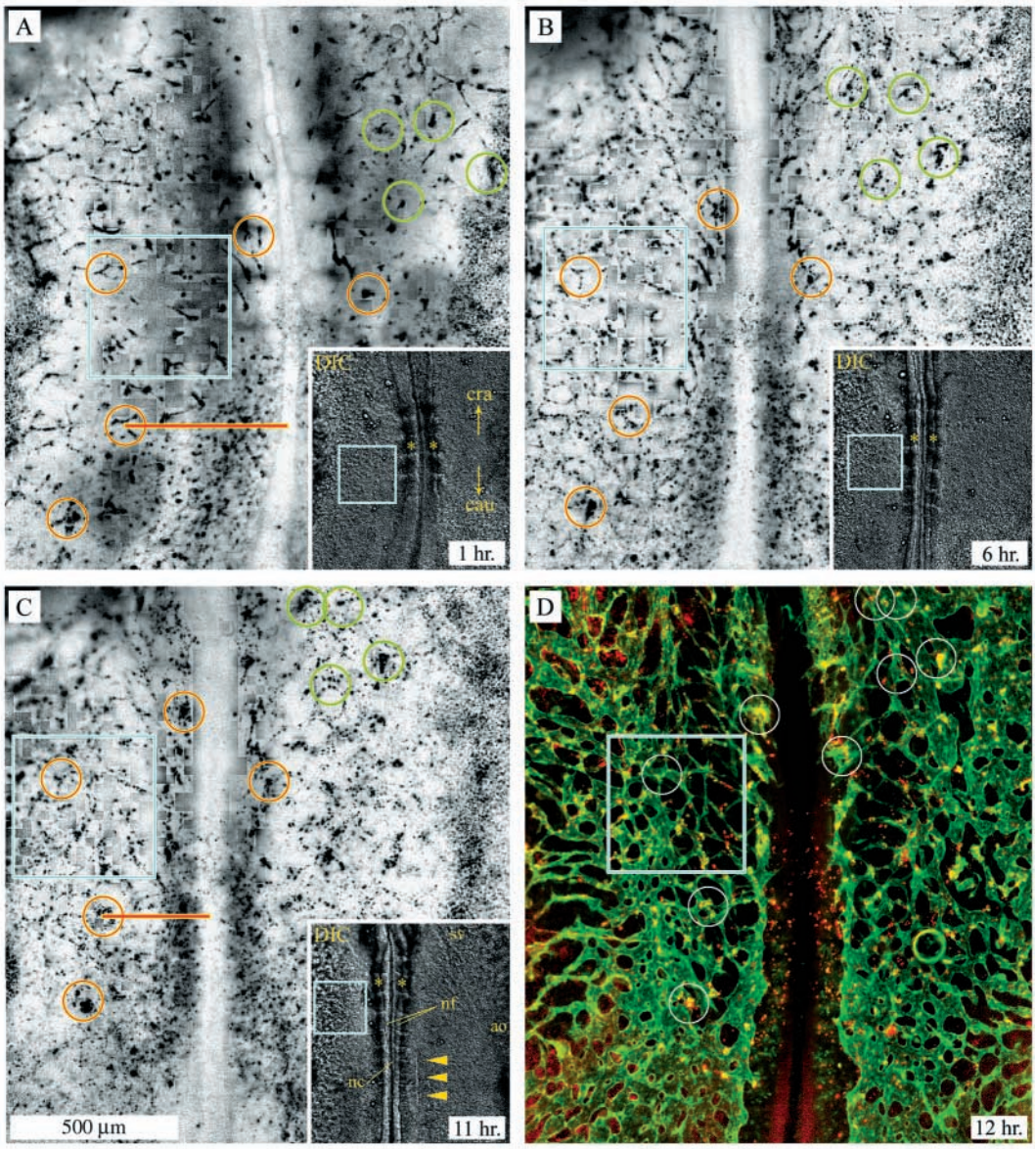

Fig. 1. Stages of early vasculogenesis. (A-C) Taken from Movie 1 at http://dev.biologists.org/supplemental. Changes in the Cy3-QH1 pulse labeled primordial endothelial cell population over a 12 hour time period, with corresponding DIC images (insets). (D) The merged image of the pulse-labeled PECs (red) and the post-experimentally Cy2-QH1 labeled vasculature (green). The red and green open circles mark the same PECs and endothelial structures whose movements are followed in each panel. Note the extensive lateral-to-medial movement of those foci lying most distal to the midline axis (red lines). By comparison, those in a more proximal position show lesser displacements. The cyan colored box indicates the field that is enlarged in Fig. 2 and serves as a frame of reference between panels. The box is 400×400 μm with the upper right corner centered on the lateral edge of the third formed somite (yellow asterisks, inset), 160 μm from the midline. All images are from the ventral aspect. The yellow arrowheads in C (inset) indicate the developing pronephros. sv, sinus venosus; nf, neural folds; ao, area opaca; nc, notochord.

Online supplemental material

A number of movies can be found at http://dev.biologists.org/supplemental, each specific for one of the first six figures. In all movies, endothelial cells are labeled with Cy3-QH1 and appear white unless otherwise noted. All still images found in figures that have been taken from movies, are inverted so that the endothelial cells and structures appear as black on a white background. The normal vasculogenesis of a HH stage 8 quail embryo is shown in Movie 1, with corresponding still images found in Fig. 1. The second movie (Movie 2) contains four panels showing vasculogenesis in two normal and two LM609-perturbed embryos. Each panel represents one 400 μm × 400 μm area that was analyzed. The upper right and lower left movies are depicted with still images in Figs 2 and 6, respectively. A progression of untreated primordial endothelial cell trajectories, also shown in Fig. 3, can be found in Movie 3. Cellular extensions and retractions, at high magnification, can be observed in the three panels of Movie 4. The left panel shows the DIC image while the middle panel displays the Cy3-QH1 pulse-labeled cells in black. The third panel is a composite of the epifluorescence (red) and DIC images. The last movie (Movie 5) displays how introduction of LM609 perturbs normal vasculogenesis in a stage 8 quail embryo. For a more complete description, including movie rates, please read the movie captions at http://dev.biologists.org/supplemental.

Results

In situ observation of endothelial cells

Vasculogenic-stage quail embryos were microinjected with a ‘pulse’ of Cy3-QH1, an antibody specific for quail vascular endothelium (Pardanaud et al., 1987), and subsequently monitored by scanning time-lapse microscopy over a 10- to 12-hour period. The resulting images were aligned such that the notochord and the intersomitic clefts remained stationary. Therefore, each reported movement, unless stated otherwise, occurs relative to these anatomical reference points. Furthermore, owing to the availability of images from multiple focal planes, no object is lost or rendered out of focus.

The labeled extracellular QH1 epitopes were largely preserved during the recorded time period (Fig. 1; see Movie 1 at http://dev.biologists.org/supplemental) (see also Czirok

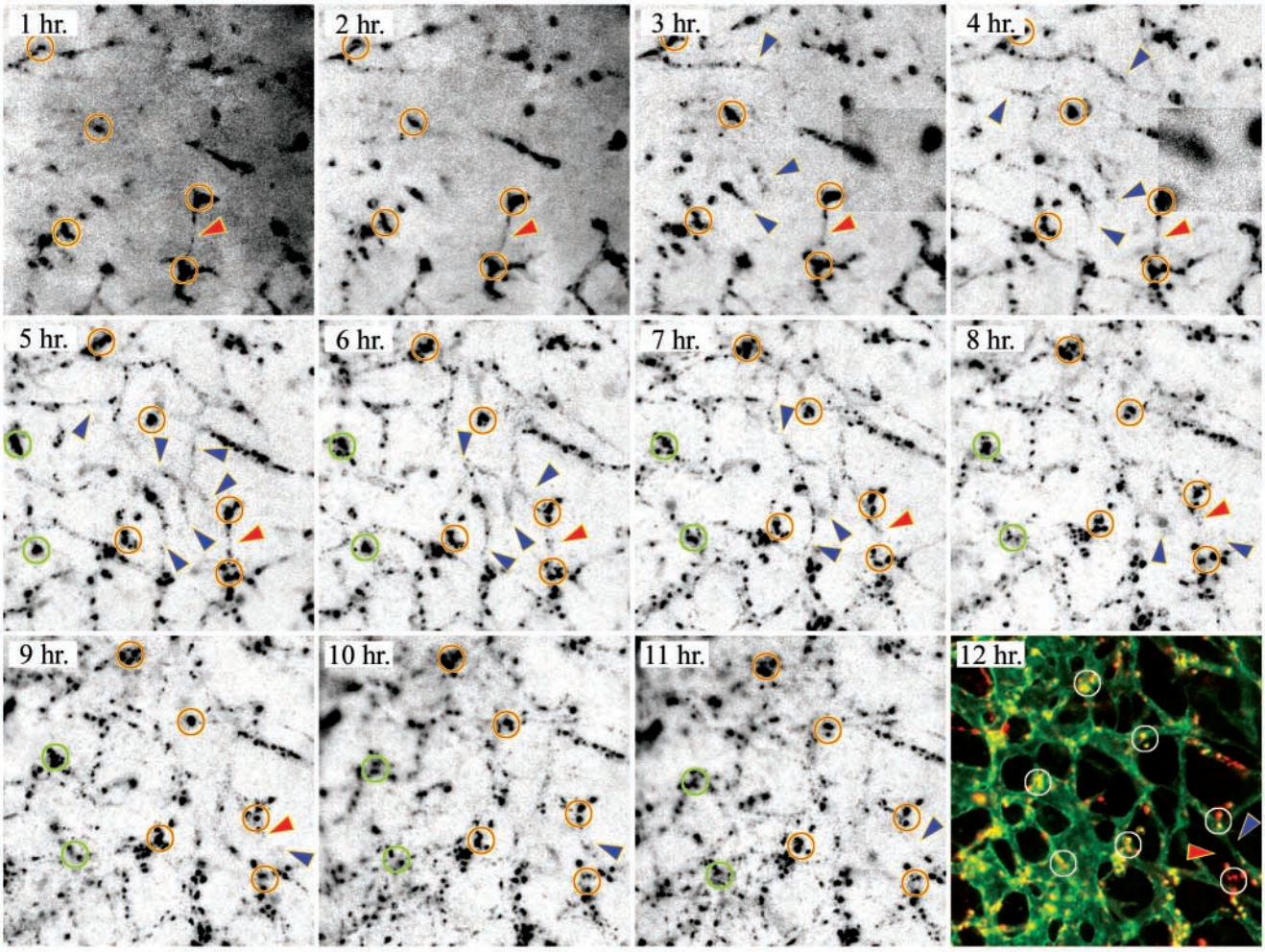

Fig. 2. Cell dynamics establishing the primary vascular plexus. Time points 1-11 show the cell configurations, at hour intervals, within the area delineated by the cyan colored box in Fig. 1. Each panel represents a 400×400 μm area enlarged from individual frames in Movie 1, and are shown in Movie 2 (see http://dev.biologists.org/supplemental). As a reference, the upper right-hand corner is centered on the lateral edge of the third somite pair 160 μm from the midline. The final panel is a merged image composed of the Cy3-QH1, experimental PEC label (red) and the post-experimental labeling of the vasculature using Cy2-QH1 (green). The open circles enclose the same endothelial structures on each panel to ease following movements. Note the lateral-to-medial movement of all denoted PECs. Green circles represent new features entering the field of view from a lateral position. Blue arrowheads indicate new cellular extensions and connections with existing polygonal structures. The red arrowheads represent retractions of vascular cords. In the last panel, a red arrowhead indicates where one connection once existed between two of the circled areas. In addition, some vasculature is formed (green) that is not recorded (red/yellow).

et al., 2002). A terminal QH1 immunolabeling at 12 hours, with a different fluorochrome (Cy2), was performed after fixation of the recorded specimen allowing the comparison of the final vascular structure with its pulse-labeled component. As Fig. 1D demonstrates, the pulse-labeled cells are randomly distributed in the final vascular structure. The relatively low concentration of pulse-labeled cells demonstrates the importance of new endothelial cell recruitment during incubation, most notably in caudal regions.

The binding of QH1 antibodies to endothelial cell-surface epitopes does not cause any detectable perturbation. Indeed, the final vascular pattern exhibited by QH1-injected embryos is not distinguishable from the vascular patterns observed in control-injected embryos or embryos that develop in ovo. We have also performed labeling with QH1 Fab fragments – such embryos are indistinguishable from embryos labeled with intact QH1 IgG except that there is a diminution in the fluorescence staining intensity (data not shown).

QH1 staining pattern

Images acquired during the first 3 hours of recording show the ‘clearing’ of QH1 antibody, manifested as the disappearance of diffuse background fluorescence (Fig. 2; see Movie 2 at http://dev.biologists.org/supplemental). QH1 homogenously stains endothelial structures for the ensuing 3-4 hours, after which time the immunofluorescence becomes punctate. Most $QH1^+$ foci initially appear as fine granular structures that originate from much larger patches of fluorescence. The median distance between neighboring foci is 10 μm, and most pairs of adjacent foci move at least 25 μm apart during the observation period.

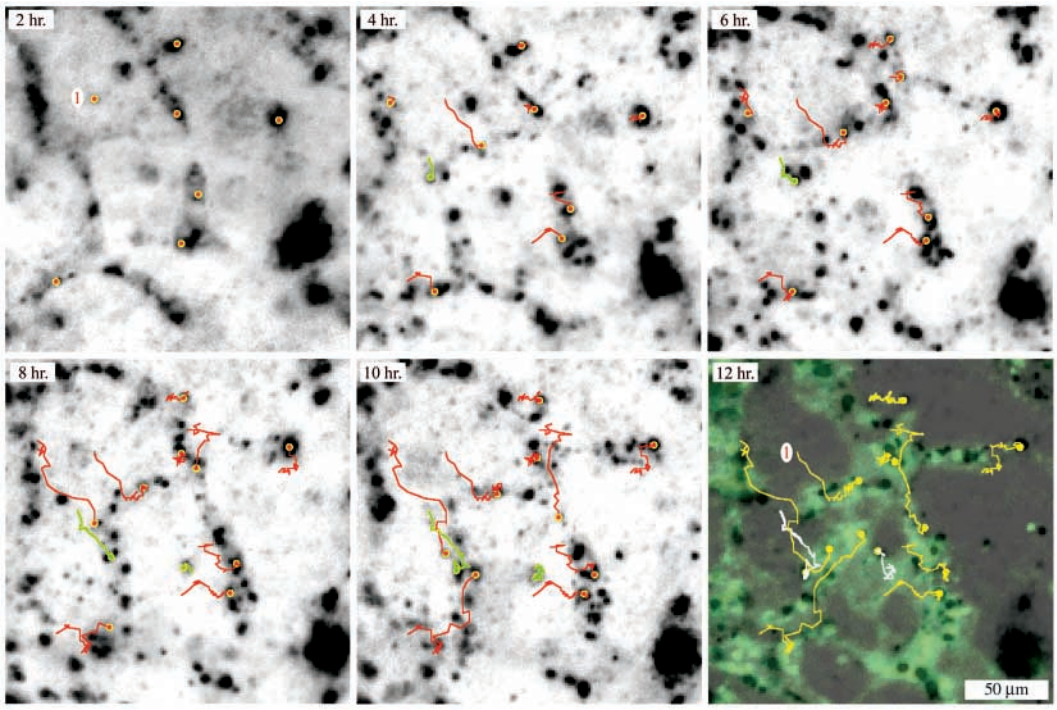

Fig. 3. Trajectories of individual primordial endothelial cells, relative to the surrounding vascular structures. Each panel is a 200×200 μm area with the embryonic midline on the right, encompassing a 10 hour period of normal development (see Movie 3 at http://dev.biologists.org/supplemental). Circles highlighted by yellow indicate the current position of representative PECs; lines show their trajectory up to the corresponding time point. Red and green are used to distinguish medially and laterally oriented motion, respectively. Even with the subtraction of the medial vascular drift, there is a heavily favored lateral-to-medial cell migration. In the final panel (12 hours), the experimentally labeled PECs (black) and cell trajectories (yellow or white) overlay the post-experimentally labeled vasculature (green). PEC #1 first appears in an avascular zone and quickly migrates to a chord structure.

Hierarchy of vasculogenic events

The primary vascular plexus is created from a combination of processes, each operating on different length scales. Accordingly, we distinguish: (1) tissue deformations that passively convect PECs as the embryonic plate folds and elongates; (2) 'vascular drift', an ordered medial movement of the entire vasculature; (3) structural rearrangement of formed vascular polygons; (4) PEC migration along existing endothelial cord structures; and (5) cellular extensions/retractions across avascular zones that form or remove links within the network. In the following we investigate each in more detail.

Tissue-scale processes

In early vertebrate embryos, vasculogenesis occurs contemporaneously with major morphogenic processes that profoundly influence the vascular pattern. This is most clearly visible at the anterior intestinal portal (AIP), where its regression is closely coupled to endocardium formation (data not shown). Here, we restrict our analysis to regions where such gross deformations do not occur: 400×400 μm areas were selected lateral to somites 3-6 at a distance of 160 μm from the embryonic axis (cyan colored boxes in Figs 1 and 5). These areas are represented at higher temporal and spatial resolution in Figs 2 and 6, respectively. These regions are distant from both the AIP and Hensen's node, sites of profound tissue deformations, and exhibit representative endothelial cell motility including vascular drift and cellular protrusive activity.

The second type of motion, vascular drift, refers to the highly correlated movement of endothelial structures, which initially may not be interconnected. This drift occurs in the lateral-to-medial direction throughout the entire area pellucida (Figs 1 and 2; see Movie 1 and upper panels of Movie 2 at http://dev.biologists.org/supplemental). As vascular polygons approach the midline where the dorsal aortae are forming, the motion decreases resulting in an accumulation of PECs.

Dynamics of cell assemblies

The tissue-scale movements described above are usually associated with structural rearrangements in the vascular network. The most frequent rearrangement is vascular fusion, whereby distinct endothelial tubes fuse to form a common sinus. This process is clearly shown in Figs 1 and 5, where the vascular structures marked by green circles approach each other and coalesce to form a nascent sinus venosus (see Movie 5 at http://dev.biologists.org/supplemental). Vascular fusion also occurs during the formation of the dorsal aortae.

Cell migration

Local trajectories of individual PECs can be established relative to the surrounding vascular network by subtracting vascular drift (Fig. 3). Each fluorescent foci can be traced back either to a cluster of endothelial cells or to an avascular area, where PECs appear de novo. These newly appearing cells move quickly until their incorporation into an existing vascular structure (PEC #1, Fig. 3). Once part of a vascular cord, PEC speed is usually reduced, and when moving, PECs remain in close vicinity of other endothelial cells.

There is a significant variation of motile activity within the endothelial cell population, as the varying trajectory behaviors demonstrate (Fig. 3; see Movie 3 at http://dev.biologists.org/supplemental). The median PEC velocity is 5 μm/hour, but a few cells move with speeds up to 40 μm/hour. Most PECs

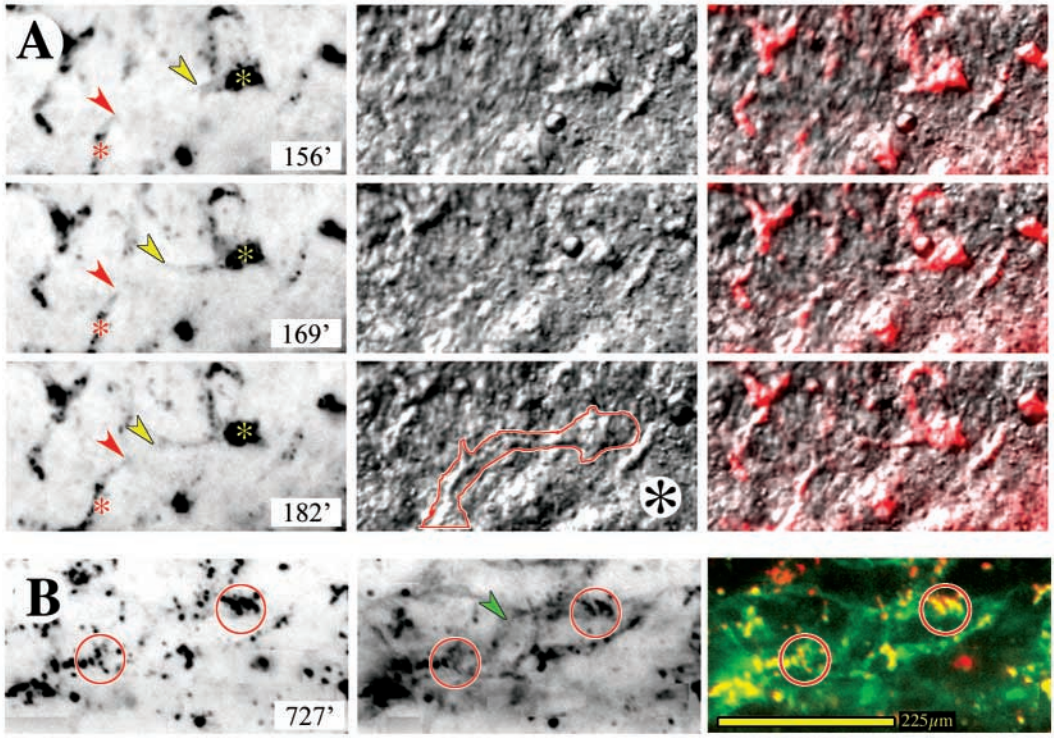

Fig. 4. High-resolution dynamics of protrusive activity. Movie 4 (see http://dev.biologists.org/supplemental) shows the extension and retraction of cellular protrusions at high magnification over a 104 minute time interval beginning 2 hours and 10 minutes into the recording. (A) Three time points from Movie 4. The left column shows QH1 experimentally labeled PECs, the middle column depicts the corresponding DIC images and the right column is a composite of the two. Red and yellow asterisks denote the relatively fixed position of two neighboring endothelial cell clusters – the two asterisks do not move substantially during the 26 minutes. By contrast, the corresponding red and yellow arrowheads indicate the presumed tips of two cell protrusions – note that these protrusions converge over the 26 minute interval. Their contact at 182 minutes is marked by a red outline on the image denoted by a black asterisk. The corresponding composite image, on the right, demonstrates that the DIC feature outlined in red is labeled with the QH1 antibody. (B) The post-experimental labeling of the same field at 12 hours and 7 minutes (727′). The left image is the experimental QH1 labeled cells, while the middle frame displays the post-experimental QH1 vasculature. After 12 hours, the original features in A (asterisks) have moved slightly, but are traceable to the positions of the red circles (see Movie 4). The green arrowhead in the middle frame points out the continuity of contact between the endothelial cell clusters. The frame on the right shows the combined fluorescence from QH1 injected 12 hours earlier in red (or yellow), and the post-fixation QH1 fluorescence labeling in green (or yellow), yellow indicates positions of overlap. Scale bar: 225 μm. The time of image acquisition is shown in the lower corner of each epifluorescence frame.

move on the vascular network from a lateral position to a more medial one.

Cell protrusions

Cells, exploring their environment, form extensions or 'sprout' into avascular zones. These protrusions can contact other extensions or endothelial cords, thereby creating new connections and vertices in the primary vascular pattern (Fig. 2, blue arrowheads). Conversely, existing cell-cell connections are also observed to retract (Fig. 2, red arrowheads). The frequency of protrusion formation is observed to diminish over time.

Higher temporal and spatial resolution reveals the creation of new connections between two adjacent endothelial cell clusters (Fig. 4; see Movie 4 at http://dev.biologists.org/supplemental). Cell protrusions can extend at a rate of 2 μm/minute into the surrounding avascular area, where they can bend, further elongate or retract. A stabilized protrusion may later be reinforced by subsequent addition of cells. No correlation between the direction of protrusive activity and the position of neighboring cell clusters was recognized, suggesting a random directionality of protrusions.

Perturbation of αvβ3 integrin function

To determine the effects of αvβ3 integrin on vasculogenic dynamics, experiments were performed in the presence of LM609 (an αvβ3 inhibitor) or, as a control, a non-function blocking antibody to the integrin αv subunit (MAB1953Z). In agreement with earlier findings (Drake et al., 1995), the presence of LM609 results in vascular malformations, most notably, unconnected endothelial cell clusters and disruption of the dorsal aortae (Fig. 5D). As the time-lapse data reveal (Figs 5 and 6; see Movie 5 and lower panels of Movie 2 at http://dev.biologists.org/supplemental), these defects are the end result of abnormal vascular cell behavior in areas exposed to LM609 – while other embryogenic events proceed normally (somitogenesis, regression of Hensen's node and the AIP, and elongation of the embryo along the anteroposterior axis).

Qualitative characterization of vascular dynamics revealed a substantial effect in the LM609-injected embryos (see Table 1). To allow a quantitative assay of LM609-induced changes, embryos injected at the five-somite stage were selected for further analysis. Introduction of LM609 was found to substantially reduce vascular drift (Figs 5 and 7). The cumulative displacement of an unperturbed vascular pattern can typically approach 80 μm within a 10-hour time period with the intensity of this movement diminishing with time. The presence of LM609 strongly reduces these displacements, especially early on (88% at 4-hour time point). As a consequence, fewer PECs arrive at medial positions, thus disrupting vascular fusion at the dorsal aortae, while fusion clearly continues at the more cranial sinus venosus.

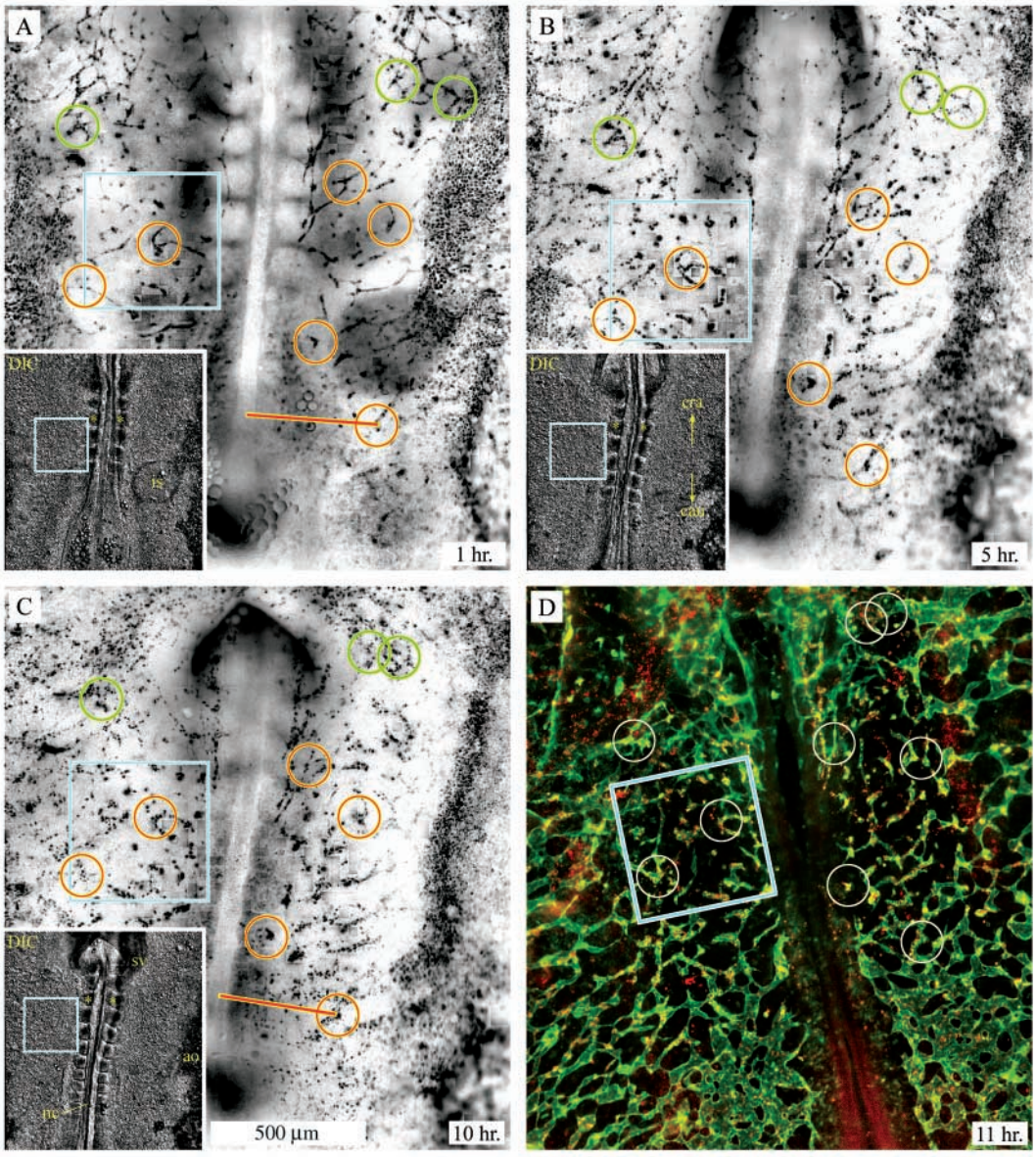

Fig. 5. Blocking αvβ3 integrin activity disrupts early vasculogenesis. (A-C) Taken from Movie 5 (see http://dev.biologists.org/supplemental), show changes in endothelial structures over a 10 hour period within an embryo injected with LM609, an αvβ3 blocking antibody. (D) The merged image of the Cy3-QH1, pulse labeled (red) and the post-experimentally labeled vasculature (green). In D, the disruption of the dorsal aortae and the polygonal network is clearly visible (see Fig. 1 as a normal reference). Clusters of vascular endothelial cells, characteristic for earlier stages (A in Figs 1 and 5) persist, lacking protrusions and connections. The red and green open circles indicate the same endothelial structures on each panel. By comparing with Fig. 1, a substantial reduction in the lateral-to-medial vascular drift is observed (red bars). The vasculature marked by green open circles is fused while being drawn into the developing endocardium. This motion seems to be unaffected by LM609 exposure. The cyan box delineates the field that is enlarged in Fig. 6 and serves as a frame of reference between panels. The position of this area as well as the markers, with the exception of one (is, injection site), is the same as in Fig. 1.

Normal and perturbed PEC trajectories, which are established relative to surrounding vascular structures, were compared by two complementary statistical approaches.

(1) To characterize the ratio of the slow versus fast moving cells within the population, the velocity distribution function was determined (Fig. 8). The average motility in LM609 treated embryos exhibited a significant, 30% reduction (P<0.05). The shape of the distribution, however, remained similar to an exponential distribution, indicating a continuous spectrum of cell activity (Czirok et al., 1998; Upadhyaya et al., 2001).

(2) To characterize the directedness of the trajectories, average displacements were calculated for a series of time intervals with increasing length (Fig. 9). For a cell population undergoing pure random movement, these curves would follow a square root-like behavior, while for highly directed motility, the displacement is proportional to the time elapsed (Stokes et al., 1991). Blocking αvβ3 integrin activity results in a significant, 40% reduction (P<0.05) in the average migration distances, but does not change the overall shape of the curves. Both treated and non-treated cell populations exhibit persistent

Table 1. Developmental stage-resolved endothelial cell motility in control and anti-αvβ3 injected embryos

	Relative cell motility					
	Non-injected		Anti-αv		Anti-αvβ3	
	+	–	+	–	+	–
S(i)=4	10		3		3	
S(i)=5	8		8		1	6
S(i)=6	3	3	4	3		3
S(i)=7		3		2		3
Total	21	6	15	5	4	12

Embryos microinjected at HH stages 8-9 (initial somites, 4-7) with control or anti-αvβ3 antibodies were scored for cell motility by three independent observers. A plus (+) indicates the presence of cell motility lateral to the 3-6 somites; conversely, a lack of movement is represented by a minus (–). The initial number of somites, S(i), is noted at the time of injection.

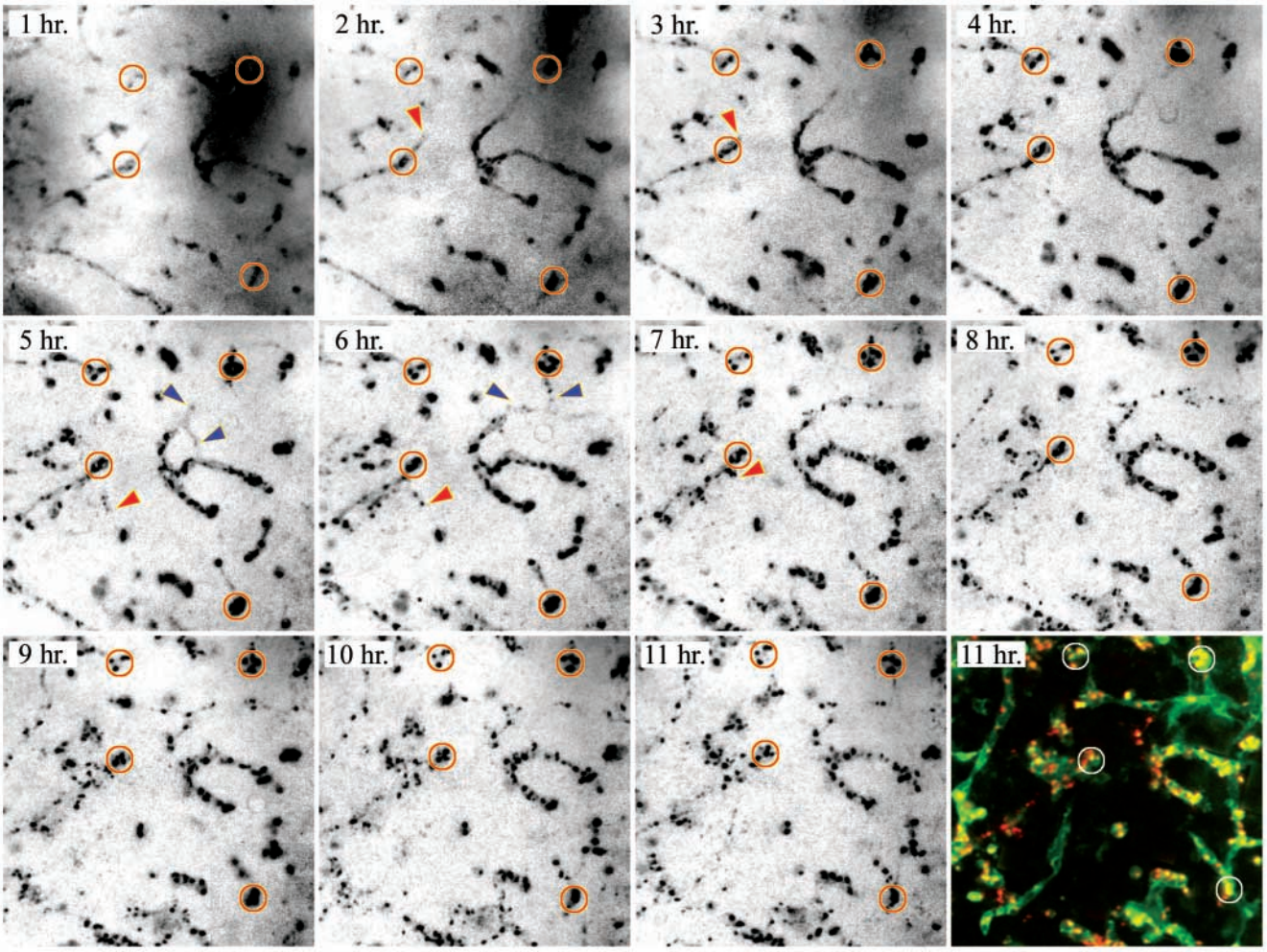

Fig. 6. Vascular cell dynamics are αvβ3 integrin dependent. Time points 1-11, enlarged from Movie 5 and displayed in the lower panels of Movie 2, show the cell configurations (at hour intervals) within the area delineated by the cyan box in Fig. 5, and thus are directly comparable in location and stages with Fig. 2. Note the minimal movement and the lack of protrusions of LM609 treated cells. The annotations are the same as in Fig. 2.

motion (Fig. 9, inset), that is, cells seldom reverse their direction of migration.

The most dramatic effect is seen in the reduction of protrusive activity that is accompanied by an increase in the retraction of protrusions (Fig. 6). Although normal embryos are characterized by an average protrusion frequency of 2.45±0.36 protrusions/hour within the selected areas, introduction of LM609 reduces this by 64% to 0.88±0.41 protrusions/hour. As a result, early clusters of endothelial cells fail to disperse into the vascular network.

In summary, normal endothelial cells exhibit local protrusive activity, motility along pre-existing polygons, engage in structural rearrangements, and have a lateral-to-medial drift similar in nature to sheet-like migration. Addition of an αvβ3 integrin inhibiting antibody most dramatically reduces endothelial cell protrusive activity and medial vascular drift. By contrast, microinjection of a non-function blocking antibody to the αv integrin subunit had no observable effect on vascular drift, PEC movement or protrusive activity at concentrations ranging from 100 to 400 ng. Similarly, in limited trials, injection of a function blocking αvβ5 integrin antibody appeared to have no effect on endothelial cell dynamics at the stages studied (P.A.R., A.C. and C.D.L., unpublished).

Discussion

The dynamics of primary vascular plexus formation is still not understood, although it has been known for nearly a century that endothelial cells differentiate from solitary angioblasts within the avian embryo (Reagan, 1915; Sabin, 1920). Committed angioblasts display a random spatial distribution within the mesoderm. No observable pre-existing pattern, at length scales comparable with those of the future vascular plexus polygons, is present (Drake et al., 1997). Thus, launching the assembly of the primordial vasculature should require substantial PEC motility. There are a number of studies that provide insight into angioblast behavior, although the properties and regulation of angioblast motility are poorly explored.

Based on an exhaustive analysis of QH1 immunostaining patterns, Coffin and Poole (Coffin and Poole, 1988) proposed

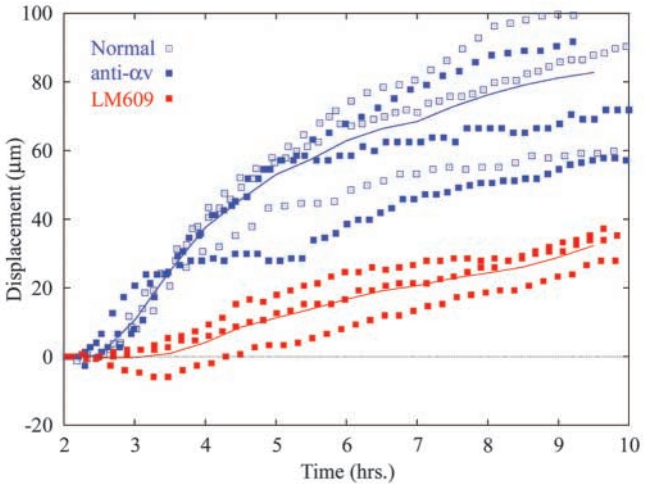

Fig. 7. Time dependence of vascular drift. Within the defined areas (cyan color boxes in Figs 1 and 5) the displacement of the entire vascular structure was determined using a frame-by-frame comparison of the fluorescence pattern. To eliminate adaptation artifacts occurring in the first hour of culture, displacements were measured from the second hour of recording. Data obtained from three normal (QH1 only), three anti-αv (QH1 plus anti-αv) and three LM609-injected (QH1 plus LM609) embryos are shown, each represented by a separate curve. Averages of control (normal and anti-αv; blue) and experimentally treated (LM609; red) embryos are shown by the unbroken lines. Positive displacement represents movement in the medial direction. Exposure to LM609 resulted in a significant 88%, 73% and 70% reduction in endothelial structure displacement at 4, 6 and 8 hour time points, respectively.

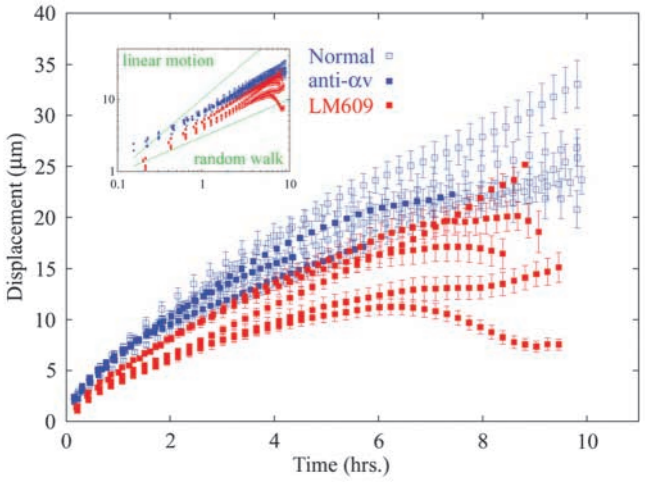

Fig. 9. Average displacements, d, of normal and LM609-perturbed primordial endothelial cells as a function of the length of time interval, τ. Each curve is calculated from the trajectories of a least 40 PECs within a lateral area from each of three normal (QH1 only), three anti-αv (QH1 plus anti-αv) and three LM609-injected embryos (QH1 plus LM609). The form of the $d(\tau)$ curve is highly characteristic for the underlying trajectories. As the plot with logarithmic scales (inset) demonstrates, the cells motility is superdiffusive and persistent (slope larger than 0.5). Blocking of the αvβ3 integrins results in a 40% reduction in the average displacements.

a medial migration of angioblasts destined to form the dorsal aortae. More recent work in zebrafish and *Xenopus*, also demonstrated medial migration of angioblasts, arising in the lateral plate mesoderm, contributing to the formation of the axial vessels (Cleaver and Krieg, 1998; Fouquet et al., 1997). In addition, chimera studies have confirmed the migratory potential of PECs. In a number of avian experiments, quail-derived graft cells were found to disperse as far as 400 μm (Klessinger and Christ, 1996), in cranial, caudal, lateral and medial directions within their host environment (Noden, 1989; Noden, 1990; Pardanaud and Dieterlen-Lievre, 1999; Poole and Coffin, 1989; Wilting et al., 1995; Wilting and Christ, 1996). Similar results were obtained with mouse-quail chimeras (Ambler et al., 2001). These studies demonstrate that grafted angioblasts are unrestrained, invasive cells capable of motility as individuals or small clusters. However, grafting experiments have the intrinsic difficulty in that subpopulations of xenograft cells may not necessarily reflect endogenous behavior, in situ. Ambler and colleagues addressed this by labeling presumptive endothelial cells by DiI injection. As was observed in chimera studies, labeled angioblasts migrated significant distances (Ambler et al., 2001).

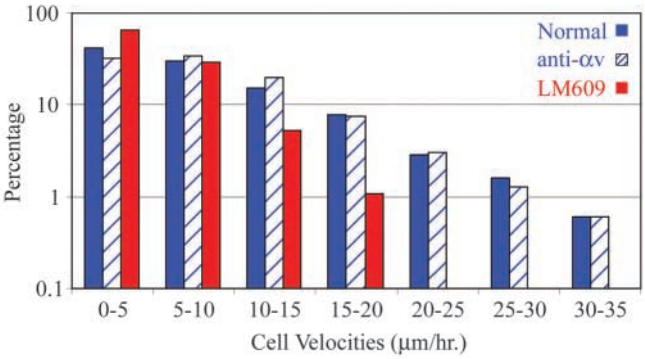

Fig. 8. Velocity distribution of primordial vascular endothelial cells. After subtraction of the vascular drift, trajectories of individual PECs were established (Fig. 3). Velocities were calculated as one hour displacements along these trajectories. The velocity distribution of normal (QH1 only), anti-αv (QH1 plus anti-αv) and LM609-perturbed (QH1 plus LM609) PECs is shown. The LM609-perturbed velocities of the PECs show a subtle increase in the slowest moving (0-5 μm/hour) population. The average motility of the population was reduced by 30%.

Observations of in vivo cell motility are becoming more common with advances in imaging technology. GFP-constructs have been used in zebrafish studies to visualize the later stage vascularization behavior of angiogenesis (Lawson and Weinstein, 2002). Unfortunately, direct motility during zebrafish vasculogenesis was not reported and, moreover, early fish vascular morphogenesis seems to be distinct from that of warm-blooded vertebrates (Weinstein, 1999). Capitalizing on the quail-specific endothelial cell surface marker, QH1, we mapped cell movements during primary quail vasculogenesis over an area encompassing virtually all of the area pellucida. In addition to sampling a wide area, our technique permits the tracking of a large population of tagged cells and the quantitative analysis of digital image files. As the size of a typical endothelial cell is in the range of 10-20 μm, it is reasonable to assume that an approximate one-to-one relationship exists between labeled cells

and QH1$^+$-foci. Thus, QH1$^+$-foci serve as useful indicators of PEC position, especially if their displacements are much larger than an average endothelial cell.

Our time-lapse data showed global medial drift of the entire vascular ensemble – a finding that directly confirms the conclusions of Coffin and Poole (Coffin and Poole, 1988). However, the extent of this motion was much larger than anticipated: not only did cells forming the dorsal aortae migrate, but the entire primordial vascular plexus translocated medially as well. The highly ordered nature of this motion was also unexpected – instead of resembling trajectories of independently migrating cells or even groups of cells, such as occurs with neural crest migration, the process more closely resembles that of cell sheet-migration, albeit a sheet containing 'void' areas. Interestingly, extracellular matrix displacement mappings also reveal similar global medial displacement tendencies (Czirok et al., 2004), presumably reflecting the global tissue deformations characteristic of gastrulation and neurulation. The finding that LM609 substantially reduces medial drift, strongly suggests that endothelium-ECM interactions are required to produce this motion. It is possible that the composite vascular network is a single structure moving within or on the ECM. Alternatively, the vascular network may be embedded within and moving in concert with other cell groups migrating medially.

We documented the motile activity of individual PECs superimposed upon tissue deformations and vascular drift. In most cases, the cells move along tracts of existing vasculature, but a few PECs sprout into avascular areas as well. The trajectory of individual motile cells is highly persistent with little frequency of direction reversal. As PECs, in the immediate vicinity, can be observed to migrate in opposite directions, this directed motility is more likely to be a cell autonomous property rather than the consequence of an external directional guidance system (i.e. no 'local' chemotactic gradient). The two types of endothelial cell motility (drift versus individual) differ mainly with respect to their substrates: while tissue-scale movement and protrusive activity is highly integrin-dependent and requires an active engagement of the ECM, PEC motility along existing vascular structures appears to rely more upon cell-cell interactions.

The LM609-induced reduction in PEC motility is reflected by the persistence of small endothelial structures and cell clusters. A cell that is associated with a small endothelial segment can migrate freely upon that structure until it attempts to venture into an avascular zone, which, in an LM609-treated environment, is largely prohibited. As LM609-perturbed cells still show persistent motion, the displacement of that cell is limited to the length of the endothelial structure to which it is confined, thus reducing both the distance migrated and the velocity of the cell.

Many investigators have shown that blocking functional αvβ3 integrins reduces vascularization. Our results now directly connect this morphological finding with the reduced motility of endothelial cells and the vascular network exposed to LM609, whether it is by physically inhibiting interactions with the matrix, altering signaling pathways or a combination of the two. Our experimental data regarding the role of αvβ3 integrins in endothelial cell dynamics seem to contradict observations obtained by mouse knock-out models (Bader et al., 1998; Hodivala-Dilke et al., 1999). The most likely explanation of this apparent contradiction is that PECs have redundant mechanisms by which they can engage the ECM and are able to exert feedback control over the expression of various integrin receptors. Therefore, fully expressed, but blocked, receptors yield remarkably different cell behaviors than a genetically missing protein.

The dynamic cell motility data allows one to refine hypotheses regarding PEC behavior during vasculogenesis. First, the motile activity and directionality of endothelial cells is strongly influenced by cell-cell interactions. Second, protrusive activity or sprouting appears to be the key mechanism used to generate new vascular cords. Third, only a small fraction of PECs exhibits this latter type of protrusive behavior. Finally, to our surprise, we failed to find any correlation between the directionality of the protrusive behavior and the position of the surrounding QH1$^+$ cell clusters. In fact, our data are consistent with protrusion formation occurring in a random fashion with no preferred direction. The detection of neighboring endothelial structures by motile endothelial cells seems to involve extended filopodia as proposed by Flamme and colleagues (Flamme et al., 1993). This type of protrusive behavior is reminiscent of 'angiogenic sprouting', a process thought to be characteristic of later vascular development. Thus, the differences between angiogenesis and vasculogenesis seem to be further blurred – not only can de novo formed PECs become incorporated into later stage angiogenic sprouts, but sprouting or protrusive activity also seems to be a fundamental process needed to generate a primary vascular plexus.

This work was supported by National Institutes of Health grant numbers 5 F32 HL68457-02 to P.A.R. and RO1 HL68855-01 to C.D.L., the G. Harold and Leila Y. Mathers Charitable Foundation to C.D.L., and the Hungarian Research Fund (OTKA T034995) to A.C. We thank Adrienn Czirok and Mike Filla for their technical assistance.

References

Ambler, C. A., Nowicki, J. L., Burke, A. C. and Bautch, V. L. (2001). Assembly of trunk and limb blood vessels involves extensive migration and vasculogenesis of somite-derived angioblasts. *Dev. Biol.* **234**, 352-364.

Bader, B. L., Rayburn, H., Crowley, D. and Hynes, R. O. (1998). Extensive vasculogenesis, angiogenesis, and organogenesis precede lethality in mice lacking all alpha v integrins. *Cell* **95**, 507-519.

Brooks, P. C., Clark, R. A. and Cheresh, D. A. (1994a). Requirement of vascular integrin alpha v beta 3 for angiogenesis. *Science* **264**, 569-571.

Brooks, P. C., Montgomery, A. M., Rosenfeld, M., Reisfeld, R. A., Hu, T., Klier, G. and Cheresh, D. A. (1994b). Integrin alpha v beta 3 antagonists promote tumor regression by inducing apoptosis of angiogenic blood vessels. *Cell* **79**, 1157-1164.

Brooks, P. C., Stromblad, S., Klemke, R., Visscher, D., Sarkar, F. H. and Cheresh, D. A. (1995). Antiintegrin alpha v beta 3 blocks human breast cancer growth and angiogenesis in human skin. *J. Clin. Invest.* **96**, 1815-1822.

Cleaver, O. and Krieg, P. A. (1998). VEGF mediates angioblast migration during development of the dorsal aorta in Xenopus. *Development* **125**, 3905-3914.

Czirok, A., Rongish, B. J. and Little, C. D. (2004). Extracellular matrix dynamics during vertebrate axis formation. *Dev. Biol.* **268**, 111-122.

Czirok, A., Rupp, P. A., Rongish, B. J. and Little, C. D. (2002). Multi-field 3D scanning light microscopy of early embryogenesis. *J. Microsc.* **206**, 209-217.

Czirok, A., Schlett, K., Madarasz, E. and Vicsek, T. (1998). Exponential distribution of locomotion activity in cell cultures. *Phy. Rev. Lett.* **81**, 3038-3041.

Davidson, L. A., Hoffstrom, B. G., Keller, R. and DeSimone, D. W. (2002). Mesendoderm extension and mantle closure in Xenopus laevis gastrulation: combined roles for integrin alpha(5)beta(1), fibronectin, and tissue geometry. *Dev. Biol.* **242**, 109-129.

Drake, C. J. and Little, C. D. (1991). Integrins play an essential role in somite adhesion to the embryonic axis. *Dev. Biol.* **143**, 418-421.

Drake, C. J. and Little, C. D. (1995). Exogenous vascular endothelial growth factor induces malformed and hyperfused vessels during embryonic neovascularization. *Proc. Natl. Acad. Sci. USA* **92**, 7657-7661.

Drake, C. J., Davis, L. A. and Little, C. D. (1992). Antibodies to beta 1-integrins cause alterations of aortic vasculogenesis, in vivo. *Dev. Dyn.* **193**, 83-91.

Drake, C. J., Cheresh, D. A. and Little, C. D. (1995). An antagonist of integrin alpha v beta 3 prevents maturation of blood vessels during embryonic neovascularization. *J. Cell Sci.* **108**, 2655-2661.

Drake, C. J., Brandt, S. J., Trusk, T. C. and Little, C. D. (1997). TAL1/SCL is expressed in endothelial progenitor cells/angioblasts and defines a dorsal-to-ventral gradient of vasculogenesis. *Dev. Biol.* **192**, 17-30.

Drake, C. J., LaRue, A., Ferrara, N. and Little, C. D. (2000). VEGF regulates cell behavior during vasculogenesis. *Dev. Biol.* **224**, 178-188.

Flamme, I., Baranowski, A. and Risau, W. (1993). A new model of vasculogenesis and angiogenesis in vitro as compared with vascular growth in the avian area vasculosa. *Anat. Rec.* **237**, 49-57.

Fouquet, B., Weinstein, B. M., Serluca, F. C. and Fishman, M. C. (1997). Vessel patterning in the embryo of the zebrafish: guidance by notochord. *Dev. Biol.* **183**, 37-48.

Hamburger, V. and Hamilton, H. L. (1951). A series of normal stages in the development of the chick embryo. *J. Morphol.* **88**, 49-92.

Hegedus, B., Czirok, A., Fazekas, I., B'Abel, T., Madar'asz, E. and Vicsek, T. (2000). Locomotion and proliferation of glioblastoma cells in vitro: statistical evaluation of videomicroscopic observations. *J. Neurosurg.* **92**, 428-434.

Hodivala-Dilke, K. M., McHugh, K. P., Tsakiris, D. A., Rayburn, H., Crowley, D., Ullman-Cullere, M., Ross, F. P., Coller, B. S., Teitelbaum, S. and Hynes, R. O. (1999). Beta3-integrin-deficient mice are a model for Glanzmann thrombasthenia showing placental defects and reduced survival. *J. Clin. Invest.* **103**, 229-238.

Keller, R., Davidson, L., Edlund, A., Elul, T., Ezin, M., Shook, D. and Skoglund, P. (2000). Mechanisms of convergence and extension by cell intercalation. *Philos. Trans. R. Soc. Lond. B Biol. Sci.* **355**, 897-922.

Klessinger, S. and Christ, B. (1996). Axial structures control laterality in the distribution pattern of endothelial cells. *Anat. Embryol.* **193**, 319-330.

Lawson, N. D. and Weinstein, B. M. (2002). In vivo imaging of embryonic vascular development using transgenic zebrafish. *Dev. Biol.* **248**, 307-318.

Little, C. D. and Drake, C. J. (2000). Whole-mount immunolabeling of embryos by microinjection. Increased detection levels of extracellular and cell surface epitopes. *Methods Mol. Biol.* **135**, 183-189.

Manoussaki, D., Lubkin, S. R., Vernon, R. B. and Murray, J. D. (1996). A mechanical model for the formation of vascular networks in vitro. *Acta Biotheor* **44**, 271-282.

Marsden, M. and DeSimone, D. W. (2001). Regulation of cell polarity, radial intercalation and epiboly in Xenopus: novel roles for integrin and fibronectin. *Development* **128**, 3635-3647.

Noden, D. M. (1989). Embryonic origins and assembly of blood vessels. *Am. Rev. Respir. Dis.* **140**, 1097-1103.

Noden, D. M. (1990). Origins and assembly of avian embryonic blood vessels. *Ann. New York Acad. Sci.* **588**, 236-249.

Pardanaud, L., Altmann, C., Kitos, P., Dieterlen-Lievre, F. and Buck, C. A. (1987). Vasculogenesis in the early quail blastodisc as studied with a monoclonal antibody recognizing endothelial cells. *Development* **100**, 339-349.

Pardanaud, L. and Dieterlen-Lievre, F. (1999). Manipulation of the angiopoietic/hemangiopoietic commitment in the avian embryo. *Development* **126**, 617-627.

Poole, T. J. and Coffin, J. D. (1989). Vasculogenesis and angiogenesis: two distinct morphogenetic mechanisms establish embryonic vascular pattern. *J. Exp. Zool.* **251**, 224-231.

Reagan, F. P. (1915). Vascularization phenomena in fragments of embryodic bodies completely isolated from yolk sac blastoderm. *Anat. Rec.* **9**, 239-241.

Rieu, J. P., Upadhyaya, A., Glazier, J. A., Ouchi, N. B. and Sawada, Y. (2000). Diffusion and deformations of single hydra cells in cellular aggregates. *Biophys. J.* **79**, 1903-1914.

Rupp, P. A., Rongish, B. J., Czirok, A. and Little, C. D. (2003). Culturing of avian embryos for time-lapse imaging. *BioTechniques* **34**, 274-278.

Sabin, F. R. (1920). Studies on the origin of the blood vessels and of red blood corpusles as seen in the living blastoderm of chick during the second day of incubation. *Carnegie Contrib. Embryo.* **9**, 215-262.

Shimizu, H., Zhang, X., Zhang, J., Leontovich, A., Fei, K., Yan, L. and Sarras, M. P., Jr (2002). Epithelial morphogenesis in hydra requires de novo expression of extracellular matrix components and matrix metalloproteinases. *Development* **129**, 1521-1532.

Stokes, C. L., Lauffenburger, D. A. and Williams, S. K. (1991). Migration of individual microvessel endothelial cells: stochastic model and parameter measurement. *J. Cell Sci.* **99**, 419-430.

Upadhyaya, A., Rieu, J. P., Glazier, J. A. and Sawada, Y. (2001). Anomalous diffusion and non-Gaussian velocity distribution of *Hydra* cells in cellular aggregates. *Physica A: Stat. Mech. Appl.* **293**, 549-558.

Vernon, R. B., Angello, J. C., Iruela-Arispe, M. L., Lane, T. F. and Sage, E. H. (1992). Reorganization of basement membrane matrices by cellular traction promotes the formation of cellular networks in vitro. *Lab. Invest.* **66**, 536-547.

Vernon, R. B., Lara, S. L., Drake, C. J., Iruela-Arispe, M. L., Angello, J. C., Little, C. D., Wight, T. N. and Sage, E. H. (1995). Organized type I collagen influences endothelial patterns during 'spontaneous angiogenesis in vitro': planar cultures as models of vascular development. *In Vitro Cell Dev. Biol. Anim.* **31**, 120-131.

Weinstein, B. M. (1999). What guides early embryonic blood vessel formation? *Dev. Dyn.* **215**, 2-11.

Wessel, G. M. and Wikramanayake, A. (1999). How to grow a gut: ontogeny of the endoderm in the sea urchin embryo. *BioEssays* **21**, 459-741.

Wilting, J., Brand-Saberi, B., Huang, R., Zhi, Q., Kontges, G., Ordahl, C. P. and Christ, B. (1995). Angiogenic potential of the avian somite. *Dev. Dyn.* **202**, 165-171.

Wilting, J. and Christ, B. (1996). Embryonic angiogenesis: a review. *Naturwissenschaften* **83**, 153-164.

Zhang, X., Fei, K., Agbas, A., Yan, L., Zhang, J., O'Reilly, B., Deutzmann, R. and Sarras, M. P., Jr (2002). Structure and function of an early divergent form of laminin in hydra: a structurally conserved ECM component that is essential for epithelial morphogenesis. *Dev. Genes Evol.* **212**, 159-172.